Oscillation frequency measurement of gaseous diffusion flames using electrostatic sensing techniques

Jiali WU[1], Yong YAN[2, *], Yonghui HU[1], Xiangchen QIAN[1], Ge ZHENG[1]

[1] School of Control and Computer Engineering, North China Electric Power University, Beijing 102206, China

[2] School of Engineering, University of Kent, Canterbury, Kent CT2 7NT, UK

* Corresponding author, Email: y.yan@kent.ac.uk

Abstract

The oscillation frequency of a burner flame is closely related to the combustion conditions and flame stability. Oscillation frequency measurement is essential for optimized operation of the combustion process. In this paper, the novel use of electrostatic sensors in conjunction with power spectral analysis is presented for the oscillation frequency measurement of a gaseous laminar diffusion flame. Experimental tests carried out on a combustion rig demonstrate that the developed system realises oscillation frequency measurement with a relative deviation from the reference value from an imaging system within ±6% over a constant fuel flow rate from 0.60 L/min to 0.80 L/min. The oscillation frequency increases with the fuel flow rate and the oscillation frequencies in different regions of the diffusion flame are similar for each fuel flow rate. Under varying fuel flow rate conditions, the system can measure the instantaneous oscillation frequency with a relative deviation from the reference value from an imaging system mostly between -10% and 0%.

Key words: *Diffusion flame; oscillation frequency; electrostatic sensor; spectral analysis; combustion monitoring.*

List of symbols:

Δq	Transferred charge (C)	R_f	Feedback resistor (Ω)
K_c	Charging efficiency	I_s	Current from the electrode (A)
C	Capacitance of the equivalent capacitor (F)	S_i	Sensor signal (V)
V	Total potential difference between the two contacting surfaces (V)	S_{sum}	Sum of sensor signals (V)
ε_0	Absolute permittivity of air (F/m)	N	Total number of sensors
A	Contact area (m^2)	F_e	Measured oscillation frequency (Hz)
z_0	Critical gap including the geometrical factors between the contact bodies (m)	F_i	Reference oscillation frequency (Hz)
d	Distance from the electrode and the flame boundary (m)	$\bar{F_e}$	Mean of the oscillation frequency (Hz)
U	Signal amplitude (V)	δ	Normalized standard deviation
V_o	Voltage output of the amplifier (V)	σ	Standard deviation

1. Introduction

Oscillatory behaviour, also named as flicker or pulsation, of a burner flame originates mainly from the Kelvin-Helmholtz type instability in the buoyancy-induced shear layer surrounding the flame surface [1, 2]. The oscillation of a flame affects the rate of air entrainment into the flame and the flame height, thus causing periodic changes in the flame structure, external shape, luminous intensity, thermoacoustics, radiation, pressure field and energy efficiency [3]. The degree of flame oscillation in the aforementioned characteristics is represented by the oscillation frequency, which is closely related to the combustion conditions and flame stability [4]. Oscillation may exist even with steady supplies of fuel and oxidizer, and cause the flame failure or flame extinction under extreme conditions [5]. An unstable flame may lead to many problems such as low combustion efficiency, high atmospheric emissions, and vibration of the furnace. Therefore, oscillation frequency measurement of a burner flame is essential for optimized operation of the combustion process.

The oscillation frequency of a laminar diffusion flame is of interest to combustion engineers as oscillations are widely encountered in small combustion systems and for the fundamental understanding of turbulent flames. In order to realize the measurement of the oscillation frequency of diffusion flames, various techniques have been developed to tackle this challenge for a number of fuels. Cetegen and Ahmed [6] measured the oscillation frequency using multiple differential pressure sensors, which detected the fluctuations in the pressure of the burner surface. The radiation emitted by the flame was also measured to determine the oscillation frequency in the literature. Jin *et al.* [7] used indium tin oxide thin-film thermocouples to measure the temperature of the combustor in a scramjet and performed time-frequency analysis to extract the combustion fluctuation features. Xu and Yan [8] adopted photovoltaic cells covering the visible and infrared spectral bands to measure the oscillation frequency of flame-radiation signals. Photodiodes were also employed to acquire the intensity fluctuation of the whole band of the flame radiation and spectral analysis was performed to extract the flame oscillation frequency [9-11]. Such detectors are simple in structure and offer online continuous measurement and can detect the flame oscillation frequency over different specific wavelengths, but they have a requirement for purging air to keep the photosensitive element clean. The beam deflection technique has also been used to measure the flame oscillation frequency for the purpose of combustion diagnosis. Gotoda *et al.* [12] used a photomultiplier to detect the light intensity change as a consequence of laser beam deflection induced by flame motion and determined the oscillation frequency via fast Fourier transform analysis. Albers and Agrawal [13] adopted quantitative rainbow schlieren deflectometry to investigate the oscillation frequency of a gas-jet diffusion flame. Ge *et al.* [14] employed a schlieren device to study periodical pulsation combustion state of the methane/oxygen laminar co-flow diffusion flame.

There have been many studies of the digital imaging technique for the monitoring of the flame oscillation frequency. Huang *et al.* [15] introduced an instrumentation system based on digital imaging for on-line continuous measurement of the flame oscillation frequency. Lu *et al.* [16] adopted a camera to capture flame images and processed the luminous intensity of individual pixels in the images to investigate the oscillatory behaviour of pulverized coal flames. Farias *et al.* [17] used a digital flame monitoring system to quantify the oscillatory behaviour of bituminous coal and wood biomass flames. However, the optical probe that transmits the flame images to the camera requires not only cooling but also purging air to prevent contamination of the objective lens by fine dust. Li *et al.* [18] measured the flame oscillation frequency using an ion current sensing method, which detected the ion generation rate in the flame. Nevertheless, the size and position of the ion probe have to be considered to minimize its intrusive disturbance to the flame, and the shape and stability of the flame are easily affected by the applied electric field.

This paper reports the novel use of electrostatic sensors for measuring the oscillation frequency of a gaseous laminar diffusion flame. Electrostatic phenomena are ubiquitous in a range of industries. Electrostatic sensors have been applied to the monitoring of various industrial processes, such as quantitative characterisation of flow in pneumatic conveyors [19] and fluidized beds [20]. Electrostatic sensors have the advantages of robustness in a harsh environment, passive sensing, structural simplicity and low maintenance requirements, thus offering a good potential for the oscillation frequency measurement of a burner flame. The presence of fine particles and dust in the combustion field, which adversely affects the operation of optical monitors based on photodiodes and digital cameras, has little impact on electrostatic sensors. In addition, passive electrostatic sensors have no requirement for the supply of an electric field which is essential for ion probes and cause little intrusive disturbance to the flame. A point to note on the developed electrostatic sensor is that it is not intended to replace other sensors, such as digital cameras and photodiodes. Instead, electrostatic sensors can be used to characterize electrical properties of a burner flame, which is desirable to obtain information complementary to optical and other measurement techniques for combustion diagnosis and achieve an in-depth understanding of the electrical properties of a burner flame.

Electrostatic sensors are, in principle, applicable to both laminar and turbulent flames because all such flames have charged species in them. However, this paper focuses on the measurements and their interpretations of oscillation frequencies of laminar diffusion flames using the proposed electrostatic sensors, because such knowledge forms an important foundation for further studies of more complex flames such as turbulent premixed flames, co-firing flames, oxyfuel flames etc. The electrostatic sensor placed around the flame detects the dynamic properties of the flame through electrostatic induction and charge transfer. The flame oscillation frequency is determined through power spectral analysis of the sensor signal. The fundamental sensing principle and sensor design are included, in addition to the implementation and practical evaluation of the system under controlled laboratory conditions.

2. Measurement principle and sensor design

2.1. Sensing principle

Chemi-ionization reactions in a burner flame have sufficient exotherm to ionize the reaction products, thereby generating ions and free electrons [21, 22]. The elementary reaction responsible for ionization in the flame is [21]:

$$CH + O \rightarrow CHO^{+} + e^{-} \tag{1}$$

H_3O^+ is the dominant ionic species, which is produced by the following charge transfer reaction [22]:

$$CHO^{+} + H_2O \rightarrow H_3O^{+} + CO \tag{2}$$

where CHO^+ is quickly consumed by H_2O. Reaction (2) is much speedier than reaction (1), i.e. CHO^+ ions are destroyed faster than they are produced [23]. Some charged soot particles are also produced in a flame by thermal ionization [24]. Since a burner flame contains charged species such as free electrons, ions and soot, they are electrically conductive [21].

Fig. 1 shows the general principle of the electrostatic sensor for oscillation frequency measurement. An exposed electrode is placed around the flame to detect the surface charges on the electrode, and sense the flame movement through electrostatic induction and charge transfer. When the free electrons, ions and charged particles around the flame are in contact with the surface of the exposed electrode, charges will be transferred to the electrode. Meanwhile, with the space charges moving within and around the flame, induced charges are produced on the electrode surface. In previous studies [25], it was found that the unipolar signal from the electrode is generated through transferred charge since the flame as an integral whole is electrically neutral. The quantity of transferred charges on the electrode is dependent on various factors, for example, the burner type, fuel type, types of charged species and the variation of the flame shape. The change in the concentration of charged species is small for fixed test conditions. However, the periodic formation, upward propagation and shedding of the toroidal vortices surrounding the flame induced by buoyancy convection cause the flame oscillation and a periodic change in the flame shape. The spatial charge density around the electrode varies with the flame shape, i.e. the distance from the flame boundary to the electrode, which leads to the variation in the amount of charge transferred on the electrode.

However, the process of charge transfer resulting from the contact between the charged elements in the flame and the electrode is very complex. Some fundamental issues on the mechanism of charge transfer remain to be resolved, such as the type of transferred charge species and the prediction of direction and magnitude of charge transfer [26]. According to a condenser model [27], the contact region between a particle and an electrode is taken as a capacitor and the potential difference between the two contacting surfaces is the electromotive force for charge transfer. In the condenser model the transferred charge Δq is represented by:

$$\Delta q = K_c C V \tag{3}$$

where K_c is the charging efficiency, C is the capacitance of the equivalent capacitor, and V is the total potential difference between the two contacting surfaces. The capacitance C can be calculated from:

$$C = \frac{\varepsilon_0 A}{z_0} \tag{4}$$

where ε_0 is the absolute permittivity of air, A is the contact area and z_0 is the critical gap including the geometrical factors between the contact bodies.

Although the quantity of the transferred charge is unpredictable, it depends on the distance from the flame boundary to the sensor [25]. In response to the fluctuation in flame shape, the exposed electrode generates a current signal. Since the original current signal from the electrode is very weak, a signal conditioning module is required. The magnitude of the sensor signal represents the amount of charges transferred to the electrode, also reflecting the distance from the electrode to the flame boundary. Because of the complexity of the charge generation and distribution, it is difficult to build the analytical relation between the signal amplitude and the distance. However, the relationship between the signal amplitude and the distance can be determined through a fitted equation [25] obtained through exponential regression analysis, which is expressed as:

$$d = p_1 exp(-p_2 U) + p_3 exp(-p_4 U) \tag{5}$$

where p_1, p_2, p_3 and p_4 are factors associated with the fuel attributes and the type of the burner, U the average signal amplitude and d the distance. Therefore, the oscillatory behaviour of the flame can be obtained by spectral analysis of the sensor signal. A point to note is that this paper aims to measure the flame oscillation frequency, which is little dependent upon the signal amplitude.

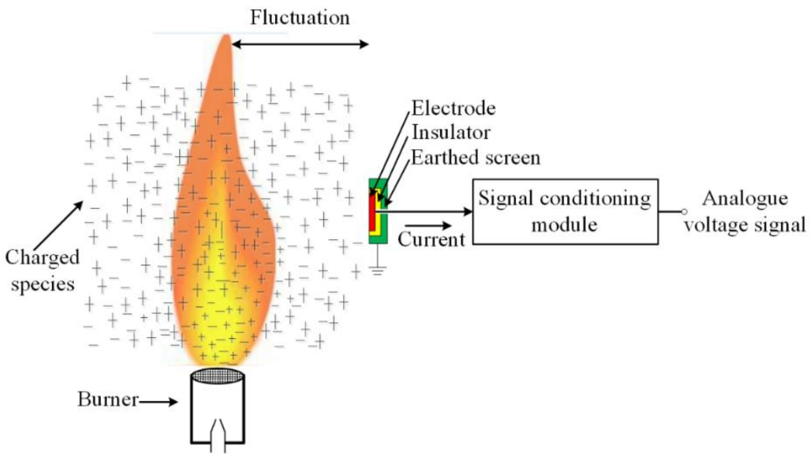

Fig. 1. General sensing principle of the electrostatic sensor.

2.2. Signal conditioning

The signal conditioning module includes three consecutive stages, which are constructed with AD8604, a wideband rail-to-rail operational amplifier. The first stage of the signal conditioning module is a trans-resistance amplifier, as shown in Fig. 2. The voltage output V_O of the amplifier is given by:

$$V_O = -I_S R_f \tag{6}$$

where R_f is the feedback resistor determining the transimpedance gain and I_s the weak current from the electrode. The value of the feedback resistor is 10 MΩ. The second stage in the signal conditioning module is a non-inverting amplifier with a voltage gain of 10. The main frequency components of the sensor signal are no greater than 30 Hz [25, 28]. The third stage is a Sallen-Key low-pass filter which cuts off unwanted noise greater than 48 Hz. Detailed information about the sensors has been reported elsewhere [23].

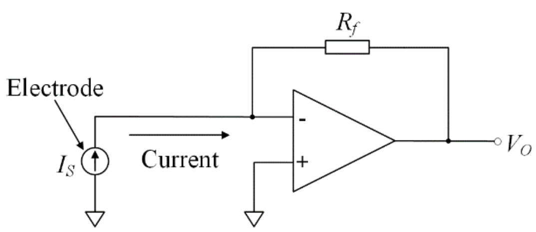

Fig. 2. Trans-resistance amplifier.

Fig. 3 shows a block diagram of the signal acquisition and subsequent analysis in the oscillation frequency measurement system. The signal acquisition is performed by a data acquisition card and the sampling frequency is set to 250 Hz. Power spectral analysis of the sensor signal is carried out to acquire its frequency components. The oscillation frequency measurement of diffusion flames has been studied by many researchers through digital imaging and image analysis [5, 15]. It was found that a diffusion flame contains a main frequency component and the variation of the radiation intensity is primarily related to the fluctuation in the flame shape. Therefore, in this paper, the dominant frequency corresponding to the maximum peak in the power spectrum is regarded as the oscillation frequency of the diffusion flame.

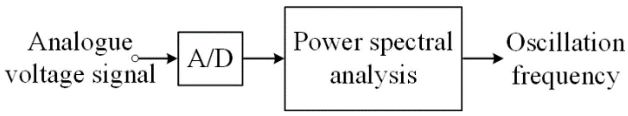

Fig. 3. Block diagram of the signal acquisition and subsequent analysis in the oscillation frequency measurement system.

2.3. Sensor design

For many applications, a single electrostatic sensor is sufficient to measure the flame oscillation frequency. For methane-fired diffusion flames, there has been limited research on the measurement of oscillation frequency in different regions. The measurement of the oscillation frequency in different regions of a diffusion flame is desirable for comprehensive investigations into the oscillatory characteristics of the flame. In order to quantify the oscillation frequencies in different regions of the diffusion flame, an array of electrostatic sensors arranged linearly along the burner axis is employed in this particular study. Fig. 4 shows the design of the electrostatic sensor array, an array of 20 strip-shaped electrodes with an axial width of 3 mm and a length of 20 mm are housed in an earthed screen (only six electrodes are drawn in Fig. 4 to avoid duplication). The electrodes are evenly spaced with a spacing of 10 mm. The vertical span of the sensor array is the same as the height of the flame to verify its feasibility. The electrodes are supported by a grounding screen to eliminate electromagnetic interference. The metal electrodes and quartz insulators meet the requirement of high-temperature resistant sensors.

The sum of the signals from the electrostatic sensor array can be adopted to indicate the total amount of transferred charges from the flame and thus the overall fluctuation of the flame shape, which is expressed as

$$S_{sum} = \sum_{i=1}^{N} S_i(t) \tag{7}$$

where $S_i\,(t)$ (i= 1, 2, …, N) denotes the i^{th} sensor signal and N is the total number of sensors that are used to encompass the flame height. The power spectrum of S_{sum} is analysed to acquire the information about the overall movement of the flame. A comparison between the overall and local dynamic properties of the flame can be thus conducted.

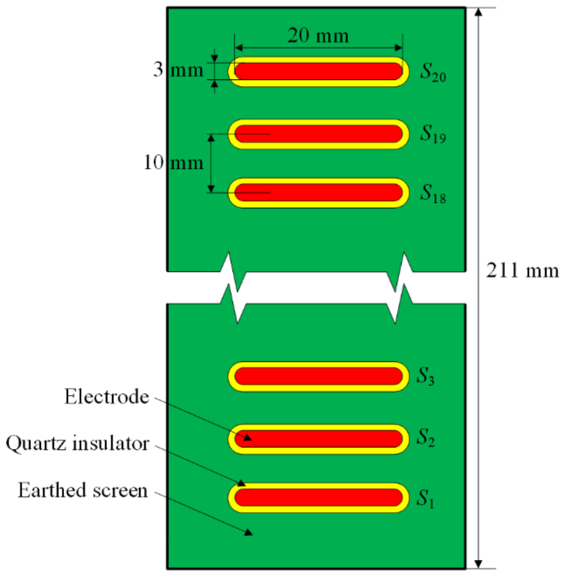

Fig. 4. Structure of the electrostatic sensor array.

3. Experiments and results

3.1. Experimental conditions

To evaluate the proposed methodology, experimental tests were carried out on a gas-fired combustion rig. Fig. 5(a) illustrates the layout of the test rig. A methane gas cylinder supplies the fuel at a maximum flow rate of 2 L/min. For a diffusion flame, the change in the fuel flowrate leads to the variation in the jet velocity of the fuel, and then affects the rate of chemical reactions and buoyancy convection, and hence the oscillation of the flame. The fuel flow rate is therefore varied to achieve different test conditions. The fuel flow rates are regulated by the flow controller, and measured and displayed by the flow meter. A burner that has an outer diameter of 24 mm is adopted to create diffusion flames in a combustion chamber with a length of 800 mm and a height of 700 mm. The flame is stabilized using a mesh screen installed at the burner outlet. Fig. 5(b) and (c) show the photos of the test rig together with the electrostatic sensor array and signal conditioning module, respectively. The array is mounted on a support frame, allowing the adjustment of the distance from the flame to the electrode. The reference oscillation frequency is obtained using a digital camera (Photron, FASTCAM Mini UX50), which acquires the flame images at a rate of 250 frames per second and with a resolution of 1280 (H) $\times$ 1024 (V). The flame intensity, which equals the sum of the pixel grey values in the image, is deemed to a reference signal. The measured oscillation frequencies in different regions are compared against the intensity of the flame image corresponding to each electrode, which equals the sum of the pixel grey values in the segmented image and is deemed to a reference signal.

In order to verify the proposed method, it is essential to acquire the sensor signals and flame images simultaneously. Fig. 5(a) shows the arrangement of the sensor head and the imaging device. The fluctuations of the signals are related to the variations in the flame shape, i.e. the change in the distance from the flame boundary to the sensor head, and the camera can capture precisely the change of such flame boundary. The arrangement in Fig. 5(a) is therefore reasonable. The sampling frequency of flame images is the same as that of the sensor signal. Synchronous acquisitions of the sensor signals and the images were realized using a digital signal from the acquisition card which triggers the digital camera. Then, the sensor signals were fed to a host computer for the calculation of the oscillation frequency. A standard frequency-varying light source with a resolution of 1 Hz was adopted as an ideal flame light to calibrate the digital camera [29]. The frequency varied from 10 to 60 Hz with an interval of 10 Hz. Fig. 6 illustrates a direct comparison between the frequency from the imaging system and the reference frequency from the light source. The relative error of the measured frequency is found to be within ±2%. An important point to stress is that previous experimental tests have verified that the non-reactive gas flow leads to no generation of the signal from the electrostatic sensor.

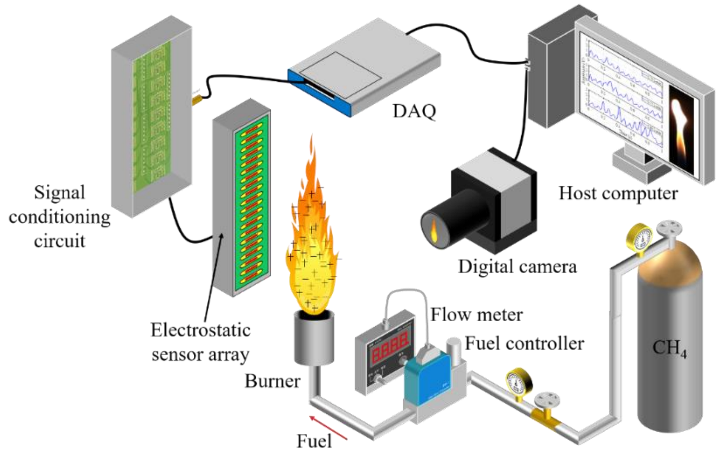

(a)

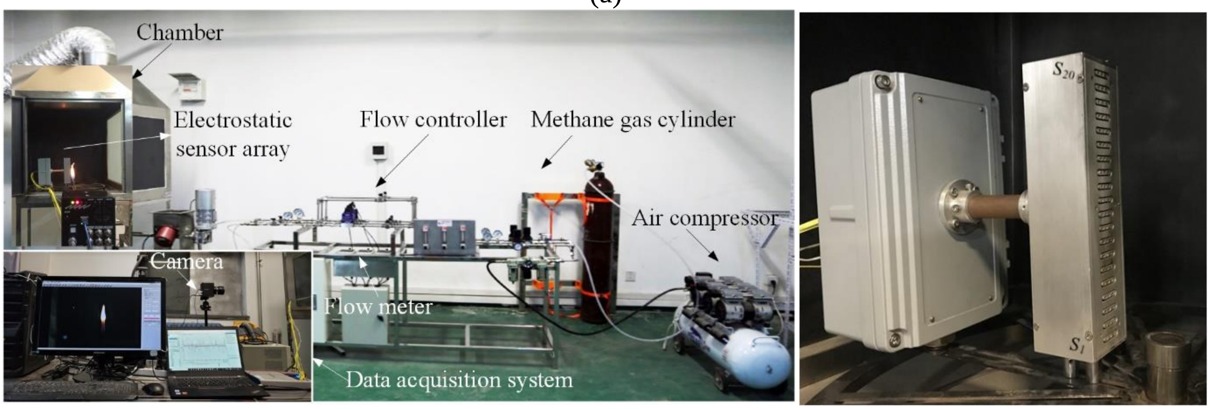

(b) (c)

Fig. 5. Experimental setup. (a) Layout of the test rig. (b) Photo of the test rig. (c) Photo of the electrostatic sensor array and signal conditioning module.

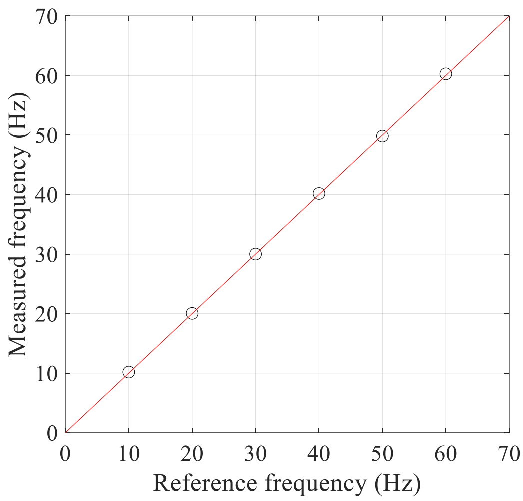

Fig. 6. Comparison between the measured frequency from the imaging system and the reference frequency.

In this study the accuracy of the measurement system is quantified in terms of relative deviation, i.e. the discrepancy between the measured and reference values:

$$D_r = \frac{F_e - F_i}{F_i} \times 100\% \tag{8}$$

where F_e and F_i are the measured and reference oscillation frequencies, respectively. The repeatability of the system is represented by the normalized standard deviation of the measured oscillation frequency [19]:

$$\delta = \frac{\sigma}{\overline{F_e}} \times 100\% \tag{9}$$

where σ and $\overline{F}_e$ are the standard deviation and mean of the oscillation frequency, respectively. Since the normalized standard deviation (δ) depends on both the repeatability of the measurement system and that of the test rig, the true repeatability of the measurement system is better than δ. A total of 25 measurements under the same test condition over a period of 100 s were acquired in each repeatability test.

3.2. Characteristics of sensor signals

3.2.1. Validation of the electrostatic sensing technique

A sequence of snapshots of a typical diffusion flame is illustrated in Fig. 7, which shows the movement of the flame during one pulsation period. The instantaneous flame images in Fig. 7 were captured from 52 to 124 ms with an interval of 4 ms. Fig. 8 shows flame images at maximum and minimum radiation intensities for four pulsation periods, which are marked as a, b, … and h. In this case, the installation distance from the sensor to the burner axis is set to 25 mm. The corresponding sum of signals from the electrostatic sensor array and grey levels of flame images are shown in Fig. 9. It can be seen that both measurements contain a significant periodic component. Scrupulous observations of such two signals and flame images in Fig. 8 show that, when the flame height peaks, the magnitude of the sensor signal and the grey level also reach maxima (moments ‘b’, ‘d’, ‘f’, and ‘h’ in Fig. 9). Such results illustrate that the electrostatic sensors can sense the change of flame shape.

Fig. 7. Flame snapshots during one period (fuel flow rate = 0.65 L/min).

(a) 52 ms (b) 104 ms (c) 124 ms (d) 180 ms (e) 196 ms (f) 252 ms (g) 272 ms (h) 332 ms

Fig. 8. Flame images at minimum and maximum radiation intensities.

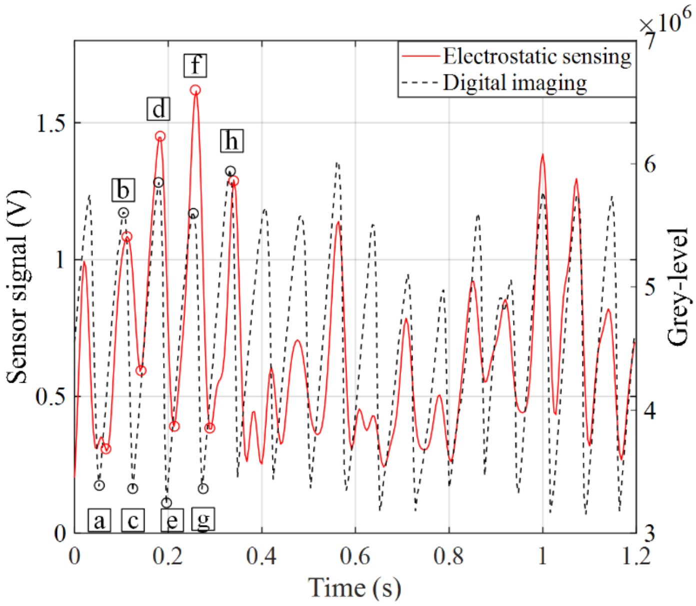

Fig. 9. Typical signals from the electrostatic sensor array and imaging system (fuel flow rate = 0.65 L/min). (a, b, … and h represent moments that the radiation intensities of flame images reach minimum and maximum for four pulsation periods, respectively)

The corresponding PSD of the sensor signal and grey levels of flame images in Fig. 9 with a duration of 5 s are depicted in Fig. 10, in which the data points are normalized to the highest peak. The frequency response of the sensor signal shows a peak at 13.4 Hz, which is identical to the result from the digital imaging system. It can be seen from Fig. 10 that there exist some frequency peaks below 2 Hz in the spectra of the two types of flame signal. Scrupulous observations of the sensor signal, flame images and grey levels show that such results are attributed to the fact that the change in the flame shape is irregular, i.e., both the peak of the sensor signal and grey level are not identical for each pulsation period. There also exist peaks located in the 20-40 Hz region in higher order harmonics of the fundamental frequency (i.e. oscillation frequency). The magnitudes of higher order harmonics are much weaker than that of the fundamental frequency. In addition, there exists a prominent spectral peak (36.2 Hz) between the 2nd and 3rd order harmonics in the PSD of the sensor signal. These frequencies peaks are much lower or higher than the measured oscillation frequency and are thus ignored in this study. It can be drawn from the results that the sensors can be used to measure the flame oscillation frequency.

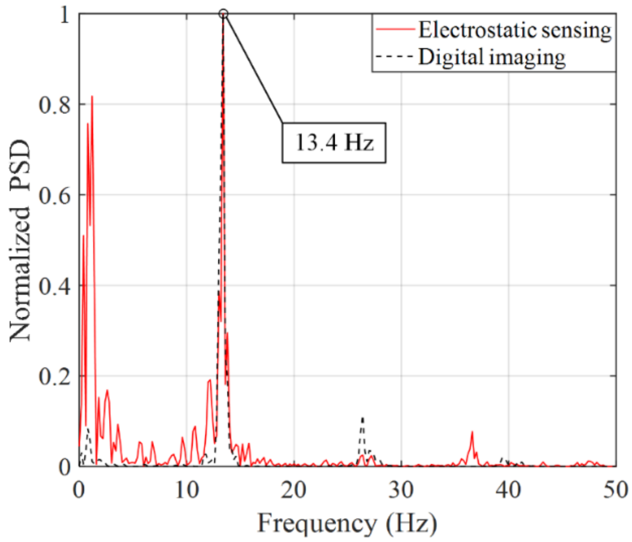

Fig. 10. Power spectra of signals in Fig. 9.

3.2.2. Effect of the sensor installation on the flame behaviour

To evaluate the influence of the sensor installation (i.e. physical presence) on the flame behaviour, a comparison between the normalized PSD of grey levels of flame images with and without the installation of electrostatic sensors at the fuel flow rate of 0.65 L/min was conducted, as shown in Fig. 11. The installation distance from the sensors to the burner axis is 25 mm. The frequency response of the grey levels with and without the electrostatic sensors yields the exactly the same peak at 13.4 Hz, illustrating that the presence of the electrostatic sensors has no effect on the behaviour of the flame. Such results illustrate that the electrostatic sensing method is capable of providing non-intrusive measurement of the oscillation frequency.

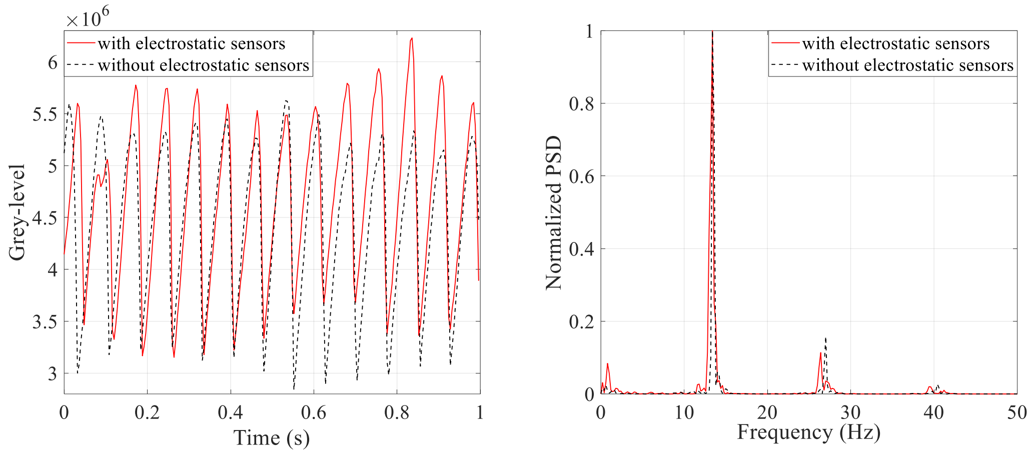

(a) (b)

Fig. 11. Grey levels of flame images and their normalized PSD with and without the installation of electrostatic sensors (fuel flow rate = 0.65 L/min). (a) Grey levels. (b) Normalized PSD.

3.2.3. Effect of the installation distance of the sensor on the measurement results

The installation distance from the sensor to the burner axis plays a significant part in the oscillation frequency measurement system. A series of experiments were thus conducted to investigate the effect of the installation distance on the measurement results, and obtain the maximum distance for valid oscillation frequency measurement at different voltage gains of the trans-resistance amplifier (Fig. 2) determined by the feedback resistor (R_f). This was achieved by gradually increasing the distance from 17 mm to 50 mm with an increment of 3 mm until the oscillation frequency became unstable or erroneous. The minimum installation distance of the sensor is 17 mm. Fig. 12 shows typical signals S_{13} and their corresponding PSD at various distances with R_f = 10 MΩ and R_f = 1 GΩ, respectively. At the higher gain, the signals at the distance smaller than 20 mm has been ignored due to signal saturation. As can be seen in Fig. 12(a), (c) that the greater the distance from the electrode and the burner axis, the weaker the output signal as less charges are transferred to the electrode surface. Observations of the power spectra of the signals at various distances have shown that the maximum distance from the sensor to the burner axis for valid oscillation frequency measurement is 35 mm and 55 mm, respectively, for R_f = 10 MΩ and R_f =1 GΩ. A point to stress is that the maximum distance may be increased further if the voltage gain of the trans-resistance amplifier in the signal conditioning module (Fig. 2) is set higher. Fig. 12(b) shows that the dominant frequency at the distance of 17 mm is smaller than under other conditions due to the fact that the closer spacing from the sensor to the flame increases the possibility of physical contact between them.

The root mean square (RMS) value of the sensor signal is employed to indicate its fluctuations, as shown in Fig. 13(a). As expected, the signal magnitude decreases with the installation distance. The measured oscillation frequencies for different distances are indicated in Fig. 13(b). It can be seen that the relative deviation of the measured frequency from the reference value increases with the distance when it is larger than 20 mm. It is because that a larger distance leads to a lower signal to noise ratio. Therefore, in consideration of the signal to noise ratio and the possibility of physical contact between the flame and the electrode, the installation distance from the sensor to the burner axis is set to 25 mm in this study. The precision of the available resistor of 1 GΩ can only reach 5% due to the limitation of the manufacturing process. In order to ensure the consistency of multiple signal conditioning channels, a feedback resistor R_f of 10 MΩ with a precision of 0.1% is used in this study.

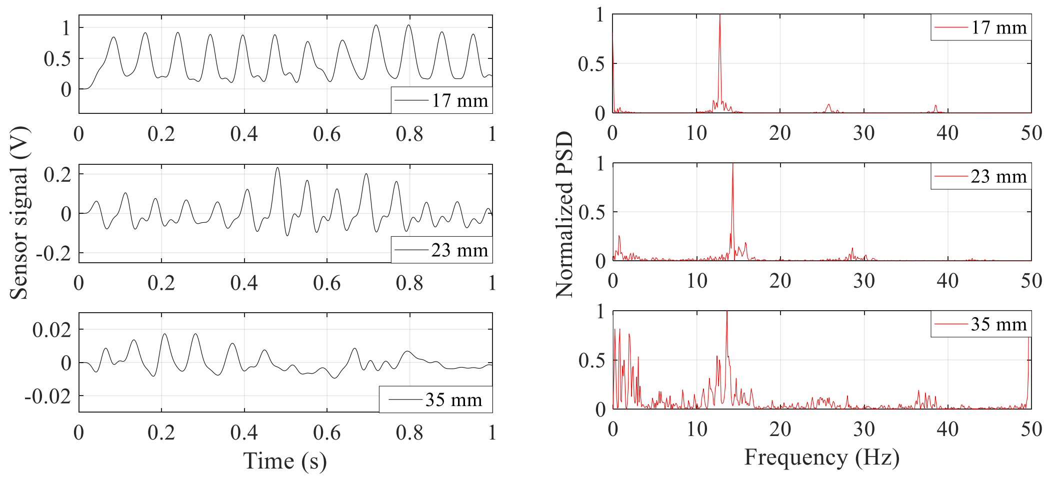

(a) (b)

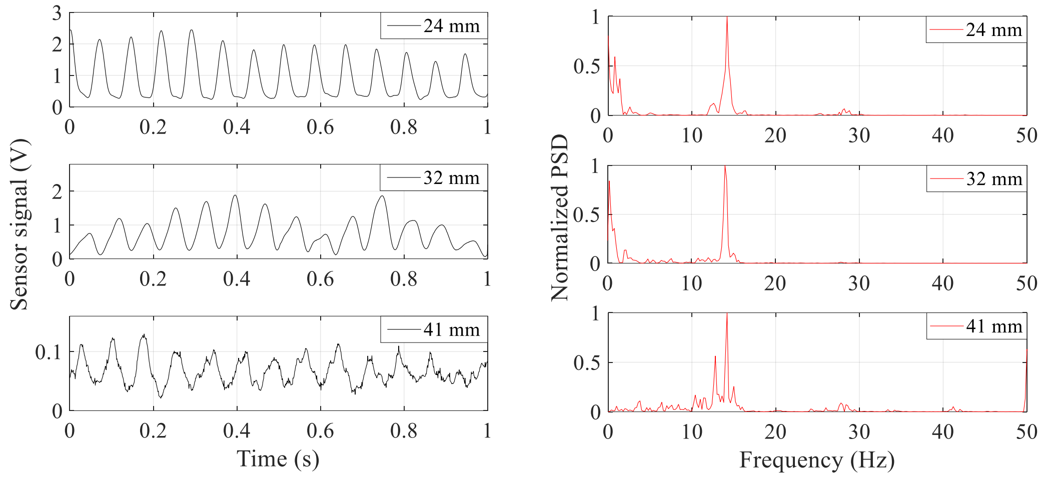

(c) (d)

Fig. 12. Sensor signals and the corresponding PSD for different installation distances. (a) Sensor signals when R_f = 10 MΩ. (b) Power spectra of signals in Fig. 12(a). (c) Sensor signals when R_f =1 GΩ. (d) Power spectra of signals in Fig. 12(c).

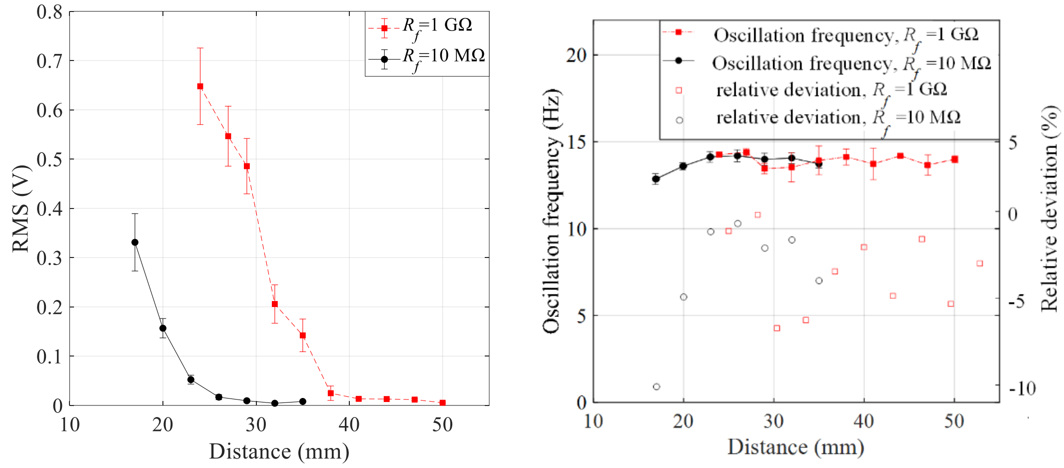

(a) (b)

Fig. 13. Signal magnitude and oscillation frequency at various installation distances. (a) Signal magnitude. (b) Oscillation frequency and its relative deviation.

3.2.4. Sensor signals

For laminar diffusion flames, experimental tests were conducted under five conditions. The fuel flow rate was varied from 0.60 L/min to 0.80 L/min (Reynolds number equals to 170-240) with an interval of 0.05 L/min. Fig. 14(a) illustrates typical signals S_7, S_9, S_{11}, S_{13} and grey level signals when the fuel flow rate is 0.70 L/min. As can be seen from Fig. 5(c), sensor 1 corresponds to the flame root and sensor 20 the fame tip. At the fuel flow rate of 0.7 L/min, sensors 1 to 7 correspond to the region of the flame root. The signals S_1, S_2, …, and S_6 are similar to the signal S_7, but with a smaller amplitude, and hence not plotted. Sensors 8 to 12, situated at the middle region of the flame, and the signal waveforms exhibit similar characteristics. Sensors 13 to 17 are located in the flame tip. A point to note is that the flame height varies with time under fixed test conditions. When the fuel flow rate is 0.70 L/min, the tip of the shortest flame can reach up to sensor 13 and hence signal S_{13} is plotted. A smaller fluctuation of the amplitude was observed in both the signal S_7 and the corresponding grey level of flame images. It results from the increasing distance from the flame to the electrode and slighter fluctuation of the flame in its root region. It can be seen that signals S_9 and S_{11} and the corresponding grey level exhibit a larger amplitude because of the closer distance in the middle region. Sensor 13, situated at the flame tip, generates a signal of a much larger amplitude owing to the closer distance and significant fluctuation at the flame tip. Smaller amplitude is observed in the corresponding grey level, which is consistent with the observations in flame images. Both signals from the electrostatic sensors and the digital imaging system exhibit a clear periodicity. The corresponding normalized PSD of the signals (Fig. 14(a)) are plotted in Fig. 14(b). The flame has a main component at a comparatively lower frequency, indicating a good agreement with the flame imaging studies conducted by Huang *et. al.* [15]. A distinct peak can be seen at 13.8 Hz in the spectra of the two types of signals, demonstrating that the oscillation frequencies of the flame are similar along the burner axis. Fig. 14(b) indicates that there are more spurious peaks in the 30-40 Hz region in the signal S_7. This is because the root region where sensor 7 is located exhibits more rigorous kinetic variations in the rate of energy emission of reacting species, resulting in the existence of higher frequency components in the PSD, though this region is relatively more stable geometrically than other parts of the flame.

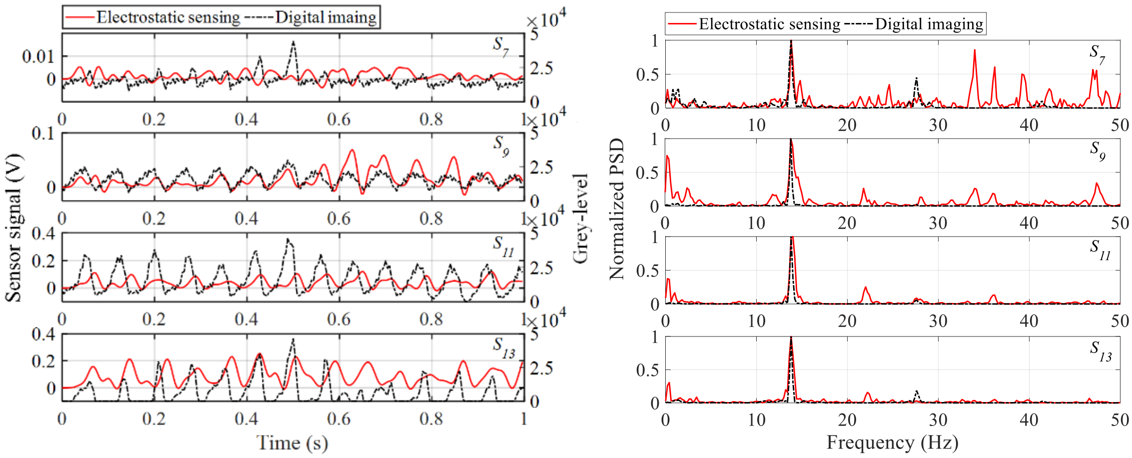

(a) (b)

Fig. 14. Typical signals from sensors 7, 9, 11, 13 and grey levels from the digital camera and the corresponding power spectra. (a) Typical signals. (b) Power spectra.

Fig. 15(a) shows the sum of signals obtained from the sensor array and grey levels at the fuel flow rate of 0.60, 0.70 and 0.80 L/min, respectively. It is clear from Fig. 15(a) that the sensor signal and the grey level of the flame images depend on the fuel flow rate. Unsurprisingly, the signal amplitude increases with the fuel flow rate, because of the increasing chemical reactions at a higher fuel flow rate and hence the resulting generation of more free electrons, ions and soot. Fig. 15(b) illustrated the corresponding power spectra of the signals and grey levels. The magnitudes of the peaks in both power spectra are almost the same.

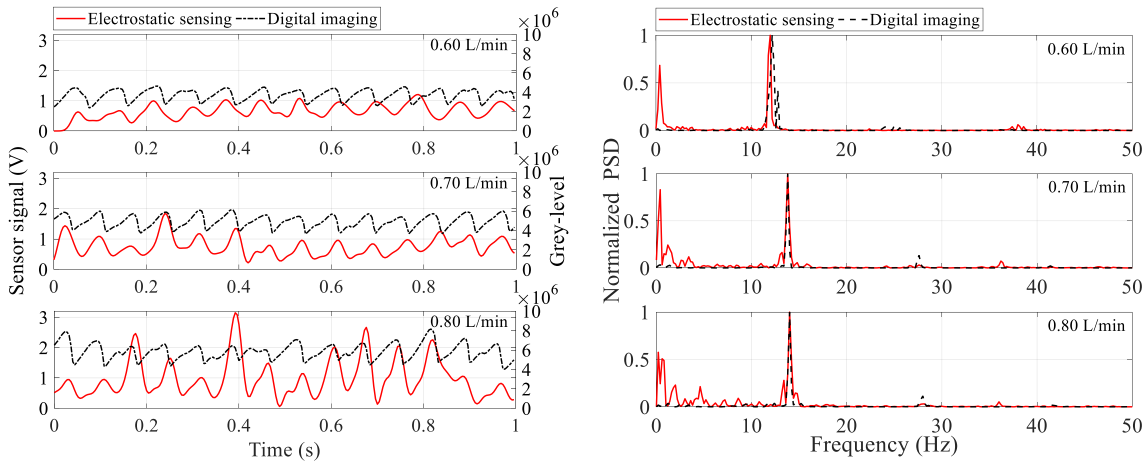

(a) (b)

Fig. 15. Typical signals from the sensor array and grey levels from the digital camera for different fuel flow rates. (a) Typical signal waveforms. (b) Power spectra of the signals.

3.3 Measurement Results

Fig. 16 shows the measurement results of oscillation frequencies in different flame regions. The measured and reference oscillation frequencies in different flame regions for various fuel flow rates are depicted in Fig. 16(a). The height of the measured flame increase with the fuel flow rate, but within a narrow range. For a diffusion flame, the flame tip can reach up to the 13^{th} electrode (fuel flow rate = 0.65 L/min). In order to compare the variation of the oscillation frequency with the flame height for different fuel flow rates, the signals from 13 sensors, i.e. sensors 1 to 13, for each fuel flow rate are used to obtain the measurement results. As shown in Fig. 16(a), the measured and reference oscillation frequencies yield a similar trend. It can be observed that the oscillation frequencies in different regions of the diffusion flame vary within a small margin for each fuel flow rate, indicating that the oscillation of the flame shape along the longitudinal direction is consistent. For the larger fuel flow rate, the oscillation frequency is mostly larger than that for the smaller one at the same flame height.

For all measured flames in this study, the flame height lower than 102.5 mm corresponds to the root and middle regions of the flame whilst that higher than 102.5 mm corresponds to the flame tip. As shown in Fig. 16(b), the relative deviation of the measured oscillation frequency from the reference value is mostly within ±5%. Normalized standard deviation of the measured oscillation frequency in different regions of the diffusion flame, as shown in Fig. 16(c), is not greater than 10% for the root and middle regions and less than 5% for the flame tip. In other words, the standard deviation of the measured oscillation frequency for the flame tip is smaller than that for the root and middle regions. This is because that the flame tip fluctuates more strongly due to aerodynamic or convective effect and then more charges are transferred on the electrode at the corresponding location owing to the closer distance and hence better signal quality. The system performs better in terms of repeatability at the flame tip because of the increased charge on the electrode.

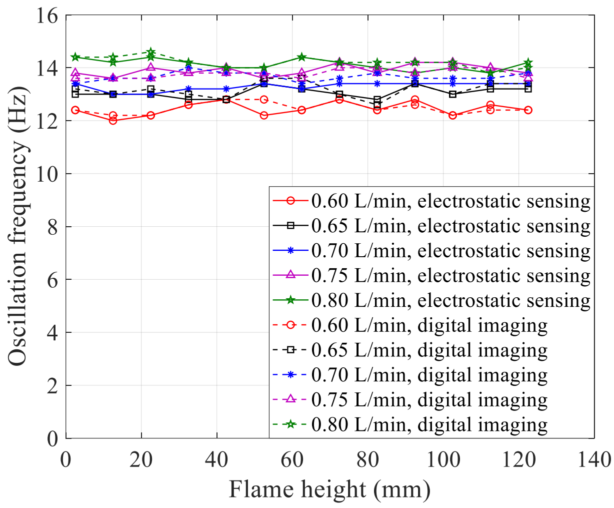

(a)

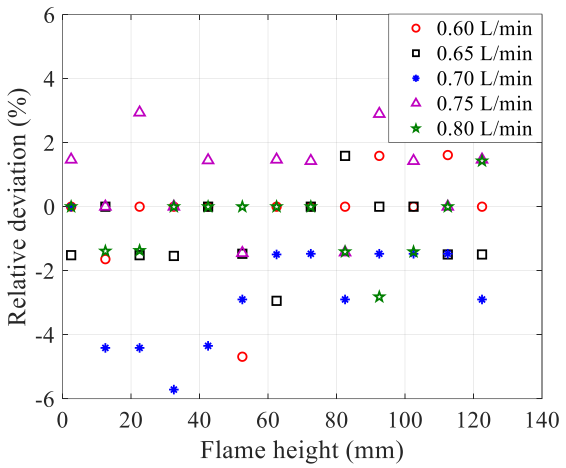

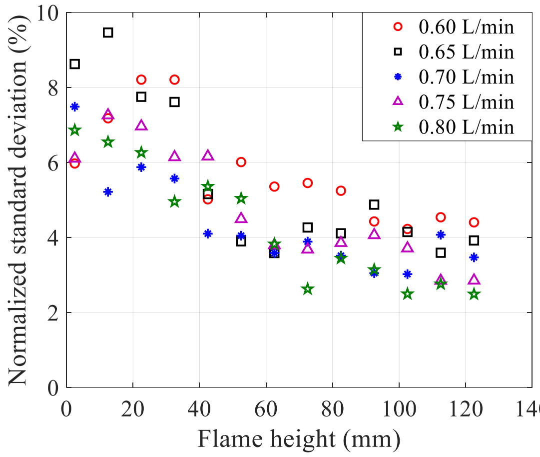

(b) (c)

Fig. 16. Measured oscillation frequencies and their deviations in different regions of the diffusion flame. (a) Comparison between the measured and reference frequencies. (b) Relative deviation of the measured oscillation frequency. (c) Normalized standard deviation of the measured oscillation frequency.

Fig. 17 shows the measured oscillation frequencies of the whole flame for different fuel flow rates. A comparison between the oscillation frequencies of the diffusion flame from the sensors and the imaging system for different fuel flow rates are depicted in Fig. 17(a). All data points in Fig. 17(a) are average values with standard deviations showed as error bars. It is obvious that both the measured and reference oscillation frequencies have an increasing trend. Fig. 17(a) indicates that the measured oscillation frequency of the whole flame is slightly smaller than the reference due to two different sensing mechanisms, and the standard deviation of the measured oscillation frequency is greater than that of the reference value. The reason for the larger standard deviation of the measured value is that the electrostatic sensing technique is slightly more sensitive to electrical interference in the environment despite the sensor is earthed properly.

Fig. 17(b) shows that the relative deviation and normalized standard deviation of the measured oscillation frequency for different fuel flow rates. The relative deviation is within -5% for the lower fuel flow rate but less than -2% for the higher fuel flow rate. The normalized standard deviation is not greater than 6% for the lower fuel flow rate, but less than 3% for the higher fuel flow rate. As the fuel flow rate increases, more charged species are generated through chemical reactions, hence the increased transferred charge on the electrode and higher signal to noise ratio, leading to smaller standard deviation of the measured value and hence better repeatability in the oscillation frequency measurement.

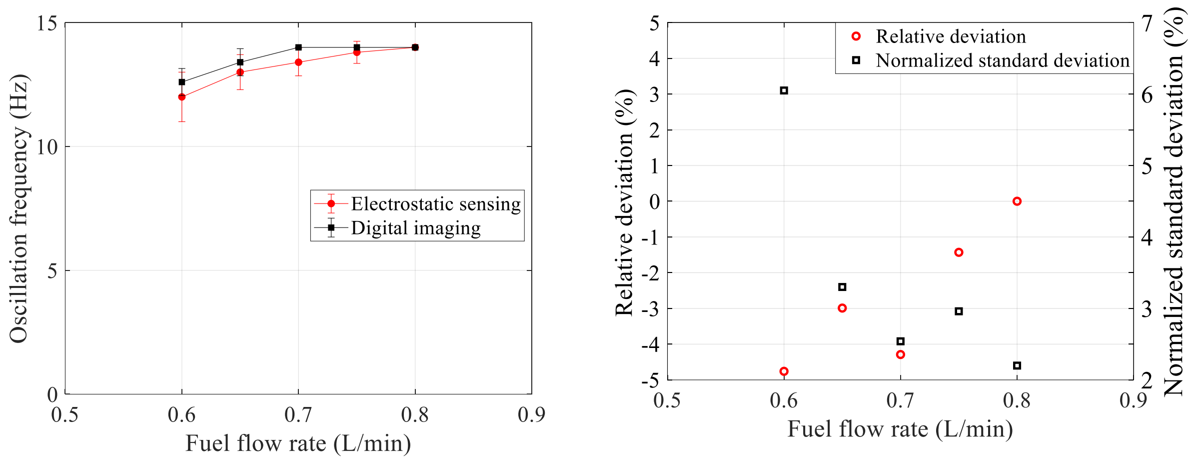

(a) (b)

Fig. 17. Measured oscillation frequencies and their deviations for different fuel flow rates. (a) Comparison between the measured and reference frequencies. (b) Relative deviation and normalized standard deviation of the measured oscillation frequency.

The performance of the developed system for the on-line continuous measurement of instantaneous oscillation frequency of a diffusion flame is verified in comparison to the reference value from the imaging system. Experimental tests were carried out by gradually increasing the fuel flow rate from 0.60 to 0.80 L/min over a period of 11 s. As can be seen in Fig. 18(a), the instantaneous oscillation frequency measured using the electrostatic sensing technique follows an increasing trend with the fuel flow rate, so does the reference from the digital imaging approach. The measured value is slightly smaller than the reference. Such results are consistent with the earlier observations (Fig. 17(a)). As can be seen in Fig. 18(b), the relative deviation is mostly between -10% and 0%. The results demonstrate that the developed electrostatic sensing system can measure the instantaneous oscillation frequency of a diffusion flame under dynamic conditions.

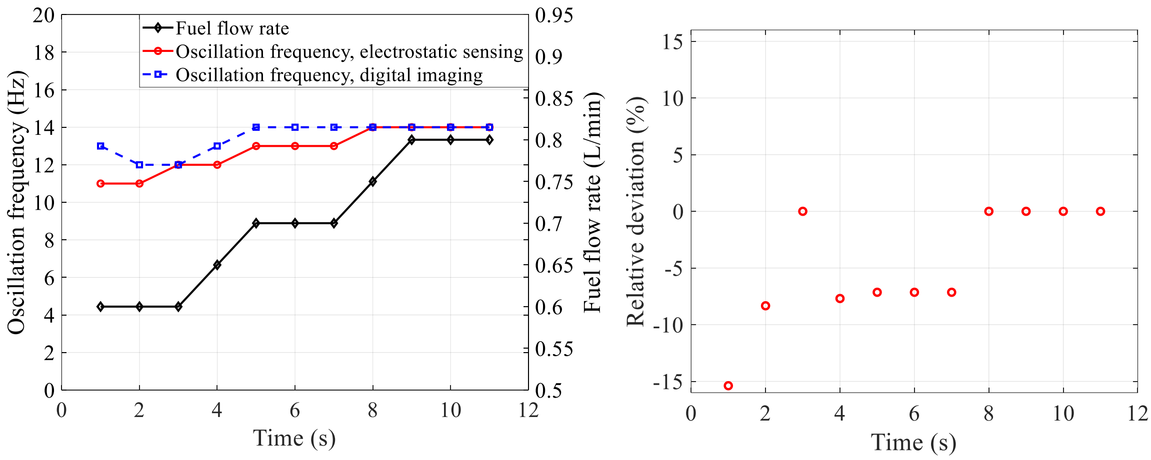

(a) (b)

Fig. 18. Results for step changes in fuel flow rates. (a) Measured and reference frequencies. (b) Relative deviation of the measured instantaneous oscillation frequency.

3.4 Discussion

Measured oscillation frequencies of different regions and the whole flame are similar for each fuel flow rate, indicating the overall and local fluctuations of the flame are consistent. The outcomes of the whole flame are more repeatable and slightly closer to the reference values in comparison with those of different regions of the diffusion flame. The measurement system performs better in terms of repeatability at the flame tip than root and middle regions.

In practical applications, either a single electrostatic sensor or an array of sensors can be used to monitor the flame and this will depend on the requirement of flame monitoring. The aforementioned results indicate that a single sensor installed at the flame tip is sufficient for the oscillation frequency measurement of a diffusion flame. An array of sensors can be used to monitor the whole flame with higher accuracy and better repeatability. However, it is essential to take the flame size into consideration to determine the number and installation location of the sensors. For example, electrostatic sensors need to be installed at the regions of interest for a large furnace flame as it is impractical to deploy the sensors that cover the whole flame.

A flame signal from an industrial furnace often has a wide frequency spectrum and the energy of the flame signal mainly distributes between 0-200 Hz [30]. In this study, the dynamic range of the oscillation frequency obtained using the electrostatic sensor array depends on the cut-off frequency of the low-pass filter. In practical applications, the cut-off frequency of the low-pass filter can be set according to the oscillation frequency of the flame. In the measurement of the flame oscillation frequency using the electrostatic sensing technique, the minimum current detectable by the electrostatic sensor can be sub-nA or even in the order of pA. In practice, the minimum concentration of charged species detectable by the electrostatic sensor depends on the size of the electrode as well as the sensitivity and performance of the signal conditioning module.

It should be pointed out that, in the case of a turbulent flame, the electrostatic sensor may not be able to detect and identify all the possible turbulences in the flame because of the finite physical dimensions of the electrode and its fundamental characteristics in electrostatic induction and charge transfer. However, the signal from the electrostatic sensor contains useful information about the fundamental oscillatory characteristics of the turbulent flame and can therefore be used for the measurement of its effective oscillation frequency.

4. Conclusions

In this paper a measurement method of the oscillation frequency of a laminar diffusion flame using electrostatic sensing and spectral analysis techniques has been presented. In order to evaluate the efficacy of the developed system, experimental tests were carried out on a combustion rig. Observations of the PSD of sensor signals have shown that the diffusion flame has a dominant frequency within a comparatively lower range, which is in agreement with the results obtained using digital imaging techniques. It has been found that the installation of electrostatic sensors around the flame has no effect on the behaviour of the flame. The system is capable of producing a valid oscillation frequency measurement as long as the installation distance of the sensor is within an effective range.

The results obtained have shown that the system performs well with a maximum relative deviation from the reference value not greater than ±6% for a fuel flow rate from 0.60 L/min to 0.80 L/min. The results have suggested that the oscillation frequency of the diffusion flame increases with the fuel flow rate. The oscillation frequencies in different regions of the diffusion flame are similar for each fuel flow rate, indicating that the oscillation of the flame shape along the longitudinal direction is consistent. The measurement system has produced more repeatable results under higher fuel flow rate conditions and at the flame tip due to increased charge on the electrode surface. Under dynamic conditions the system can measure the instantaneous oscillation frequency with a relative deviation from the reference value mostly between -10% and 0%.

Future research will be conducted to evaluate the efficacy of the developed technique for the measurement of oscillation frequencies of complex flames under a wide range of conditions.

Acknowledgments

This work was supported by the National Natural Science Foundation of China under Grant 61673170 and Grant 51827808. The IEEE Instrumentation and Measurement Society is also acknowledged for the 2018 Graduate Fellowship Award for Jiali Wu.

References

[1] J. Buckmaster and N. Peters, The infinite candle and its stability-a paradigm for flickering diffusion flames, Proc. Combust. Inst. 1986; 21: 1829–1836.

[2] J. Fang, C. Jiang, J. Wang, J. Guan, Y. Zhang and J. Wang, Oscillation frequency of buoyant diffusion flame in cross-wind. Fuel, 2016; 184: 856-863.

[3] X. Zhang, X. Fang, Y. Miao and L. Hu, Experimental study on pulsation frequency of free-, wall- and corner buoyant turbulent diffusion flames, Fuel, 2020; 276: 118022.

[4] X. Huang, T. Huang, X. Zhuo, F. Tang, L. He and J. Wen, A global model for flame pulsation frequency of buoyancy-controlled rectangular gas fuel fire with different boundaries, Fuel, 2021; 289: 119857.

[5] K. B. Sahu, A. Kundu, R. Ganguly and A. Datta, Effects of fuel type and equivalence ratios on the flickering of triple flames, Combust. Flame. 2009; 156: 484–493.

[6] B. M. Cetegen and T. A. Ahmed, Experiments on the periodic instability of buoyant plumes and pool fires, Combust. Flame. 1993; 93: 157–184.

[7] X. Jin, Y. Tian, K. Zhao, B. Ma, J. Deng and J. Luo, Experimental study on supersonic combustion fluctuation using thin-film thermocouple and time–frequency analysis, Acta Astronaut. 2021; 179: 33–41.

[8] L. Xu and Y. Yan, A new flame monitor with triple photovoltaic cells, IEEE Trans. Instrum. Meas. 2006; 55 (4): 1416–1421.

[9] N. Yilmaz, A. B. Donaldson and R. E. Lucero, Experimental study of diffusion flame oscillations and empirical correlations, Energy. Convers. Manag. 2008; 49 (11): 3287–3291.

[10] D. Durox, T. Yuan and E. Villermaux, The effect of buoyancy on flickering in diffusion flames, Combust. Sci. Technol. 1997; 124 (1): 277–294.

[11] R. Portscht, Studies on characteristic fluctuations of the flame radiation emitted by fires, Combust. Sci. Technol. 1975; 10: 73–84.

[12] H. Gotoda, T. Ueda, I. G. Shepherd and R. K. Cheng, Flame flickering frequency on a rotating Bunsen burner, Chem. Eng. Sci. 2007; 62 (6): 1753–1759.

[13] B. W. Albers and A. K. Agrawal, Schlieren analysis of an oscillating gas-jet diffusion flame, Combust. Flame. 1999; 119: 84–94.

[14] Y. Ge, S. Li and X. Wei, Combustion states distinction of the methane/oxygen laminar co-flow diffusion flame at high pressure, Fuel, 2019; 243: 221–229.

[15] Y. Huang, Y. Yan, G. Lu and A. Reed, On-line flicker measurement of gaseous flames by image processing and spectral analysis, Meas. Sci. Technol. 1999; 10: 726–733.

[16] O. M. Farias, J. Szuhánszki, G. A. Clements, B. D. Ingham, L. Ma and M. Pourkashanian, Oscillating coal and biomass flames: A spectral and digital imaging approach for air and oxyfuel conditions, Fuel Process. Technol. 2018; 173: 243–252.

[17] G. Lu, Y. Yan, M. Colechin and R. Hill, Monitoring of oscillatory characteristics of pulverized coal flames through image processing and spectral analysis, IEEE Trans. Instrum. Meas. 2006; 55 (1): 226–231.

[18] F. Li, L. Xu, Z. Cao and M. Du, A chemi-ionization processing approach for characterizing flame flickering behavior, in IEEE Instrumentation and Measurement Technology Conference, Pisa, Italy, May 2015, pp. 325–329.

[19] Y. Hu, Y. Yan, X. Qian, and W. Zhang, A comparative study of induced and transferred charges for mass flow rate measurement of pneumatically conveyed particles, Powder Technol. 2019; 356: 715–725.

[20] Z. Liu, X. T. Bi, J. R. Grace, Electrostatic charging behaviour of dielectric particles in a pressurized gas-solid fluidized bed, J Electrostat. 2010; 68: 321–327.

[21] J. Lawton and F. J. Weinburg, Electrical aspects of combustion. Oxford, U.K: Clarendon Press, 1969.

[22] H. F. Calcote, Mechanisms for the formation of ions in flames, Combust. Flame. 1957; 1: 385–403.

[23] T. Addabbo, A. Fort, M. Mugnaini, L. Parri, V. Vignoli1, M. Allegorico, M. Ruggiero and S. Cioncolini, Ion sensor based measurement systems: application to combustion monitoring in gas turbines, IEEE Trans. Instrum. Meas. 2020; 69 (4): 1474–1483.

[24] M. Balthasa, F. Mauss and H. Wang, A computational study of the thermal ionization of soot particles and its effect on their growth in laminar premixed flames, Combust. Flame. 2002; 129 (1-2): 204–216.

[25] J. Wu, Y. Yan, Y. Hu, L. Shan and W. Xu, Flame boundary measurement using an electrostatic sensor array, IEEE Trans. Instrum. Meas. 2021; 70: 2000412.

[26] F. Fotovat, X. Bi and J. R. Grace, Electrostatics in gas–solid fluidized beds: a review, Chem. Eng. Sci. 2017; 173: 303–334.

[27] S. Matsusaka, H. Maruyama, T. Matsuyama and M. Ghadiri, Triboelectric charging of powders: a review, Chem. Eng. Sci. 2010; 65: 5781–5807.

[28] J. Wu, Y. Hu, Y. Yan, X. Qian and S. Gu, Flicker measurement of burner flames through electrostatic sensing and spectral analysis, in Journal of Physics: Conference Series 1065 - the XXII World Congress of the International Measurement Confederation, Belfast, UK, September 3-6, 2018, pp. 202004.

[29] D. Sun, G. Lu, H. Zhou and Y. Yan, Flame stability monitoring and characterization through digital imaging and spectral analysis, Meas. Sci. Technol. 2011; 22 (11): 114007.

[30] L. Xu and Y. Yan, An improved algorithm for the measurement of flame oscillation frequency, IEEE Trans. Instrum. Meas. 2007; 56 (5): 2087–2093.